Modulated transverse off-plane dust-lattice wave packets in hexagonal two-dimensional dusty plasma crystals

B. Farokhi,[1] M. Shahmansouri,[1] and I. Kourakis[2]
[1]*Department of Physics, Arak University, Arak P.O. Box 38156-879, Iran*
[2]*Department of Physics and Astronomy, Centre for Plasma Physics, Queen's University Belfast,*
Belfast BT7 1NN Northern Ireland, United Kingdom

The propagation of nonlinear dust-lattice waves in a two-dimensional hexagonal crystal is investigated. Transverse (off-plane) dust grain oscillatory motion is considered in the form of a backward propagating wave packet whose linear and nonlinear characteristics are investigated. An evolution equation is obtained for the slowly varying amplitude of the first (fundamental) harmonic by making use of a two-dimensional lattice multiple scales technique. An analysis based on the continuum approximation (spatially extended excitations compared to the lattice spacing) shows that wave packets will be modulationally stable and that dark-type envelope solitons (density holes) may occur in the long wavelength region. Evidence is provided of modulational instability and of the occurrence of bright-type envelopes (pulses) at shorter wavelengths. The role of second neighbor interactions is also investigated and is shown to be rather weak in determining the modulational stability region. The effect of dissipation, assumed negligible in the algebra throughout the article, is briefly discussed. © *2009 American Institute of Physics*. [DOI: 10.1063/1.3121221]

I. INTRODUCTION

Dust crystals are space-periodic strongly coupled dusty plasma (DP) configurations (Debye lattices) which occur due to the strong electrostatic interaction between massive, heavily charged, micron-sized dust particulates (dust grains) present in a (dusty or complex) plasma.[1,2] The formation and dynamics of dust crystals have been studied in various experiments,[2–7] where dust particles were essentially created by injecting artificial microspheres, which subsequently acquire a high electron charge via inherent dynamic charging mechanisms. Such dust quasilattices typically bear a two-dimensional (2D) hexagonal structure, although various two- and three-dimensional configurations have also been reported.[2] One-dimensional (1D) dust crystals have also been fabricated in experiments by making use of appropriate confinement potentials.[6,7]

Dust lattices support a variety of linear modes of which we single out: longitudinal[8] ($\sim x$, acoustic) and a transverse[9,10] ($\sim y$, shear) in-plane, as well as a transverse (out-of-plane, inverse-optic) dust-lattice wave (DLW) mode(s). Beyond the linear regime, nonlinear effects may influence or even dominate DL dynamics if wave amplitudes become significant. This may be due to the intrinsically nonlinear character of electrostatic coupling to geometric effects (mode coupling), to interaction potential anisotropy,[11] or to sheath potential anharmonicity. The latter is of crucial importance in the vertical (off-plane) mode to be treated here; indeed, we need to stress the fact that the sheath potential, although generally believed to be parabolic,[12] may take a anharmonic form for low plasma pressure and/or density, as suggested by *ab initio* calculations[13] and also by an interpretation of earlier experimental results (see the discussion in Ref. 14 and references therein). A theoretical treatment of the *nonlinear* aspects of DL modes in 1D Yukawa crystals has

been carried out in Ref. 15, where the above aspects are incorporated in an exact nonlinear lattice model.

Recent experimental[5] and numerical (molecular dynamics)[16] investigations have established the occurrence of 2D modulated transverse dust-lattice wave (TDLW) packets moving at a negative group velocity, i.e., the wave is backward propagating. The observed waves form a 2D analog of the TDL, i.e., vertical, mode (as modeled in 1D crystals[9,10]), obeying similar qualitative physics yet substantially different dispersion laws in 2D, as discussed in Refs. 5 and 16. This *"bending mode"* was theoretically investigated in Ref. 17 in the linear region, and that linear model has succeeded in the interpretation of earlier experimental and numerical findings. Our study aims at extending those results to the weakly nonlinear regime. The results in Refs. 5, 16, and 17 are naturally recovered in our formulation below.

A well-known nonlinear effect manifested in the dynamics of waves propagating in nonlinear dispersive media is *amplitude modulation,* referring to the slow space and time variation in the wave's amplitude, which may potentially be subject to modulational instability. Modulationally unstable wave packets may either collapse in response to external perturbations or evolve toward localized structure (envelope soliton) formation due to a mutual balance between dispersion and nonlinearity. This generic mechanism is well known in various physical contexts[18,19] to be related to phase harmonic generation and energy localization via the formation of localized excitations (solitons). Analytical theories for the amplitude modulation of DLWs in 1D dust crystals due to the carrier phase self-interaction have been furnished for both longitudinal[20] and transverse (off-plane)[21] 1D modes. The nonlinear aspects of *in-plane* motion in 2D lattices were covered in Ref. 22. The investigation presented here follows

the same methodology, yet for the 2D transverse (*off-plane*) waves.

Our aim here is to study the amplitude modulation of transverse off-plane DL wave packets in 2D dusty plasma crystals. We shall investigate the occurrence of *modulational instability*, which may be viewed as a first stage triggering of the out-of-plane lattice instability observed numerically,[16(a)] presumably leading to the phase transition suggested in that reference. Modulational instability may also be the first stage of the generic (i.e., for any symmetric potential) structural instability suggested in Ref. 23. We must point out for rigor that the modulation theory employed here is a *mildly* nonlinear theory, which claims to model weak vertical displacements. The latter point justifies our choice in neglecting the coupling to in-plane dust grain motion, since we are only interested in the very first stage of the manifestation of nonlinearity in off-plane motion. A more general theory should take into account horizontal-to-vertical motion coupling and should be the subject of forthcoming work of ours. According to earlier results,[24] we will assume interactions between charged dust particles to be of the "standard" screened electrostatic (Debye–Hückel or Yukawa) type, modeled via a potential $U(r)=q^2 \exp(-r/\lambda_D)/4\pi\varepsilon_0 r$ (here λ_D denotes the effective DP Debye radius,[1] q is the dust grain charge assumed constant, and ε_0 is the permittivity of vacuum).

Our scope lies in the interpretation of dusty plasma experiments in the laboratory. However, going beyond dusty (complex) plasma physics, this work can be viewed as a fundamental investigation of nonlinear transverse motion in hexagonal crystals, which may be of relevance in other physical contexts where Debye crystals structures occur (e.g., ultracold plasmas or one-component plasmas) or in lattice theory in general.

The outline of the manuscript is as follows. The model equations of motion are derived in Sec. II and simplified by adopting a continuum approximation. The derivation of an evolution equation for the modulated wave amplitude is presented in Sec. III by assuming transverse wave propagation either along a principal axis of the hexagonal structure or perpendicular to it. The effects of second neighbor interaction (SNI) on linear and nonlinear waves are investigated in Sec. IV. The modulational stability in both cases is investigated and the results are then summarized in Sec. V.

II. ANALYTICAL MODEL AND LINEAR WAVE CHARACTERISTICS

We take into account nearest neighbor interactions (NNIs) only, i.e., each particle (m,n) interacts with the three other pairs of particles $(m\pm 1,n)$, $(m\pm 1/2, \ n-\sqrt{3}/2)$, and $(m\pm 1/2, \ n+\sqrt{3}/2)$. The physical situation considered is a 2D hexagonal crystal (assumed infinite for simplicity) consisting of negative dust grains, which are located at equidistant site a, see Fig. 1. If the particles are not at their equilibrium positions, we may define the six length variables l_1, l_2, l_3, l_4, l_5, and l_6, which represent the distances from the particle (m,n) to the nearest particles, respectively,
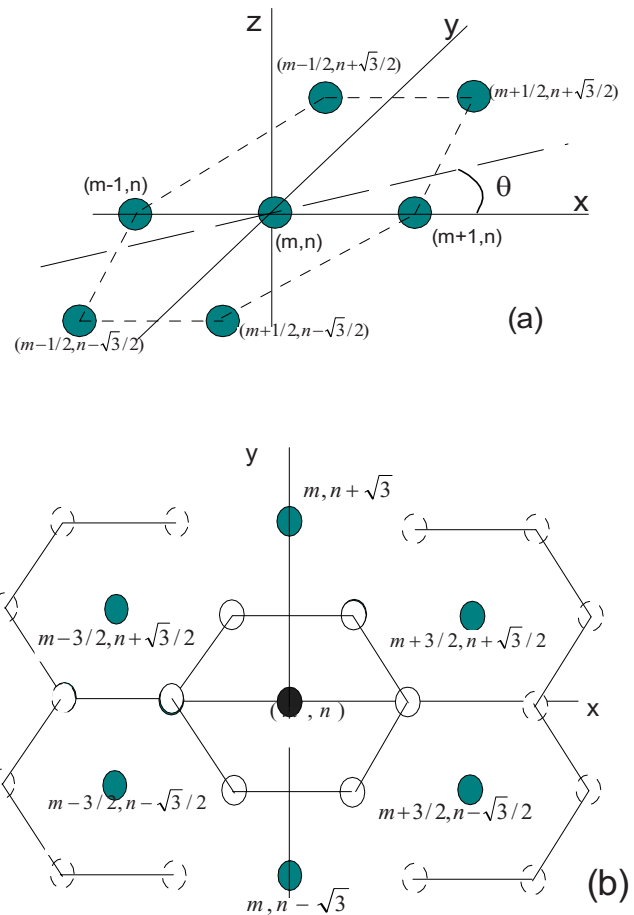

FIG. 1. (Color online) Hexagonal lattice geometry: (a) elementary cell: the six nearest particles around particle n, m; (b) the six nearest particles and the six second neighbors around particle are depicted as empty circles (forming the central hexagon) and as solid circles (forming the external hexagon), respectively.

$$l_i = \sqrt{a^2 + (\Delta z_i)^2},\tag{1}$$

where Δz_i (for $i=1,2,\ldots,6$) denotes the displacements of the respective particles from their equilibrium positions in z direction, and

$$\Delta z_1 = z_{m+1,n} - z_{m,n}, \quad \Delta z_2 = z_{m-1,n} - z_{m,n},$$

$$\Delta z_3 = z_{m+1/2,n+\sqrt{3}/2} - z_{m,n}, \quad \Delta z_4 = z_{m-1/2,n+\sqrt{3}/2} - z_{m,n}, \tag{2}$$

$$\Delta z_5 = z_{m+1/2,n-\sqrt{3}/2} - z_{m,n}, \quad \Delta z_6 = z_{m-1/2,n-\sqrt{3}/2} - z_{m,n}.$$

The equation of motion in the $z-$ direction is

$$\frac{d^2 z_{m,n}}{dt^2} + \nu \frac{dz_{m,n}}{dt} = \frac{1}{M}(F_e - Mg) + \frac{1}{M}F_z, \tag{3}$$

where the electrostatic binary interaction force in $z-$ direction F_z exerted on two grains situated at a distance r is derived from a potential function $U(r)$,

$$F_z = -\partial U(r)/\partial z, \tag{4a}$$

$$F_z = -\frac{\partial U}{\partial r}\left(\sum_{i=1}^{6}\frac{\Delta z_i}{l_i}\right) - \frac{1}{2!}\frac{\partial^2 U}{\partial r^2}\left[2\sum_{i=1}^{6}(l_i-a)\frac{\Delta z_i}{l_i}\right]$$

$$-\frac{1}{3!}\frac{\partial^3 U}{\partial r^3}\left[3\sum_{i=1}^{6}(l_i-a)^2\frac{\Delta z_i}{l_i}\right] + \cdots. \tag{4b}$$

Upon defining $G_1 = (\partial U/\partial r)|_{r=a}$, $G_2 = (\partial^2 U/\partial r^2)|_{r=a}$, and $G_3 = 1/2(\partial^3 U/\partial r^3)|_{r=a}$, we have calculated the polynomial coefficients G_1, G_2, and G_3 for the Yukawa potential.

$$G_1 = -\frac{q^2}{4\pi\varepsilon_0\lambda_D^2}(1+\kappa)\frac{\exp(-\kappa)}{\kappa^2}, \tag{5}$$

$$G_2 = \frac{q^2}{4\pi\varepsilon_0\lambda_D^3}(2+2\kappa+\kappa^2)\frac{\exp(-\kappa)}{\kappa^3}, \tag{6}$$

$$G_3 = -\frac{q^2}{4\pi\varepsilon_0\lambda_D^4}(6+6\kappa+3\kappa^2+\kappa^3)\frac{\exp(-\kappa)}{\kappa^4}, \tag{7}$$

where $\kappa = a/\lambda_D$.

We shall assume a smooth, continuous variation in the field intensity E as well as the grain charge q (which may vary due to charging processes) near the equilibrium position $z_0 = 0$. Thus, following the method and notation in Ref. 21, we will expand as

$$E(z) \approx E_0 + E_0'z + \tfrac{1}{2}E_0''z^2 + \cdots, \tag{8}$$

$$q(z) \approx q_0 + q_0'z + \tfrac{1}{2}q_0''z^2 + \cdots, \tag{9}$$

where the prime denotes differentiation with respect to z and subscript "0" denotes evaluation at $z = z_0$. Accordingly, the electric force $F_e - Mg = q(z)E(z) - Mg$ is expressed as

$$F_e(z) - Mg \approx -Mg + q_0E_0 + (q_0E_0' + q_0'E_0)z$$
$$+ 0.5(q_0E_0'' + 2q_0'E_0' + q_0''E_0)z^2 + \cdots$$
$$\approx \gamma_1 z + \gamma_2 z^2 + \gamma_3 z^3 + \cdots. \tag{10}$$

The zeroth-order term of electric force balances gravity at z_0, viz., $q_0E_0 - Mg = 0$, while the first order $-\gamma_1 = M\omega_g^2$ is the effective width of the potential well; the value of the gap frequency ω_g may either be evaluated from *ab initio* calculations or determined experimentally. For instance, in Ref. 18, the frequency ω_g is typically of order of $\omega_g/2\pi = 20$ Hz and $\gamma_2 = -\gamma_1/2$, $\gamma_3 = 0.07\gamma_1$. Now, Eq. (3) becomes

$$\ddot{z}_{m,n} + \nu\dot{z}_{m,n} = -\omega_g^2 z_{m,n} - K_1 z_{m,n}^2 - K_2 z_{m,n}^3 + \Omega^2[6z_{m,n} - z_{m+1,n} - z_{m-1,n} - z_{m+1/2,n+\sqrt{3}/2} - z_{m+1/2,n-\sqrt{3}/2} - z_{m-1/2,n+\sqrt{3}/2}$$
$$- z_{m-1/2,n-\sqrt{3}/2}] + K_3[(z_{m+1,n} - z_{m,n})^3 + (z_{m-1,n} - z_{m,n})^3 + (z_{m+1/2,n+\sqrt{3}/2} - z_{m,n})^3 + (z_{m+1/2,n-\sqrt{3}/2} - z_{m,n})^3$$
$$+ (z_{m-1/2,n+\sqrt{3}/2} - z_{m,n})^3 + (z_{m-1/2,n-\sqrt{3}/2} - z_{m,n})^3], \tag{11}$$

where

$$K_1 = -\frac{\gamma_2}{M}, \tag{12}$$

$$K_2 = -\frac{\gamma_3}{M}, \tag{13}$$

$$K_3 = \frac{G_1}{2Ma^3} - \frac{G_2}{2Ma^2}, \tag{14}$$

$$\Omega^2 = -\frac{G_1}{Ma} = \frac{q^2}{4\pi\varepsilon_0 Ma^3}(1+\kappa)\exp(-\kappa). \tag{15}$$

We note that upon keeping the single particle contributions (first line only), Eq. (11) reduces to the equation of motion suggested in Ref. 25 for dust particle motion in a anharmonic sheath potential. The remaining terms in the right-hand side are due to the electrostatic coupling, including linear (term in Ω^2) and nonlinear (term in K_3) contributions.

A. Linear dispersion relation

Waves can propagate along an arbitrary direction, which is here denoted by an angle θ, representing the angle between the wave vector k and a primitive translation vector (along the x axis), i.e., $k_x = k\cos\theta$ and $k_y = k\sin\theta$. Retaining only linear contribution in the form of "phonons" of the type

$$u_{mn} = u_0\exp[-i\omega t + ika(m\cos\theta + n\sin\theta)] + \text{c.c.},$$

we obtain an inverse-optic-mode-like dispersion relation from Eq. (11),

$$\omega^2 + i\nu\omega = \omega_g^2 - 4\Omega^2\left\{\sin^2\left[\frac{ka}{2}\cos\theta\right]\right.$$
$$+ \sin^2\left[\frac{ka}{2}\cos\left(\frac{\pi}{3}-\theta\right)\right]$$
$$\left.+ \sin^2\left[\frac{ka}{2}\cos\left(\frac{\pi}{3}+\theta\right)\right]\right\}. \tag{16}$$
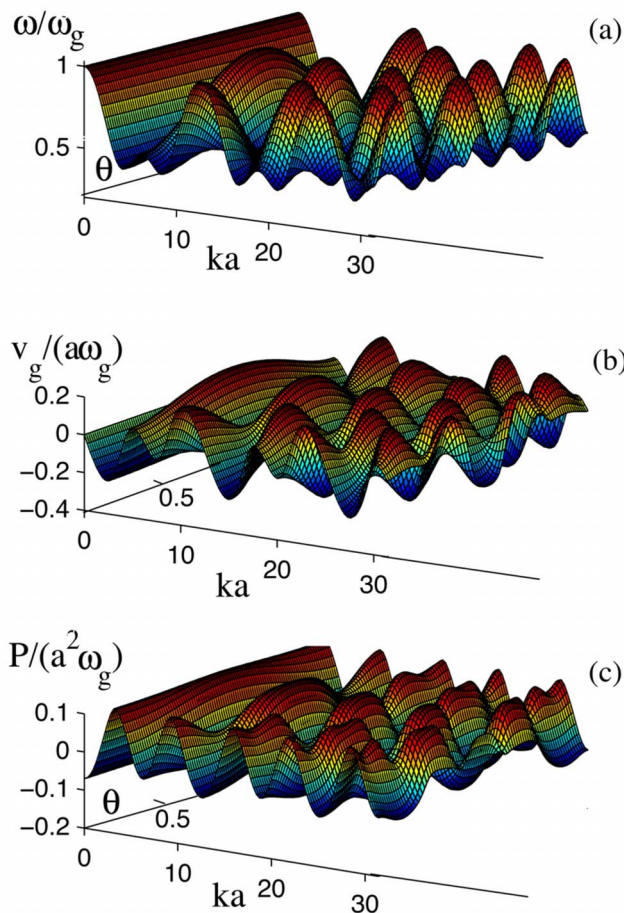
FIG. 2. (Color online) Surface plot of (a) the normalized frequency ω/ω_g, (b) the normalized group velocity $v_g = \omega'(k)$, and (c) the normalized group-velocity dispersion coefficient $P = \omega''(k)/2$ as a function of the (normalized) wave number and the angle θ. Here, we have taken $\Omega/\omega_g = 0.305$ (as in Ref. 17). Only FNI (first neighbor interaction) is taken into account here.

In the special cases $\theta = 0$ or $\theta = \pi/2$ we obtain

$$\theta = 0 : \omega^2 + i\nu\omega = \omega_g^2 - 4\Omega^2 \left\{ \sin^2\left(\frac{ka}{2}\right) + 2\,\sin^2\left(\frac{ka}{4}\right) \right\},$$

$$\text{(17a)}$$

$$\theta = \pi/2 : \omega^2 + i\nu\omega = \omega_g^2 - 8\Omega^2 \sin^2\left(\frac{\sqrt{3}ka}{4}\right).$$

$$\text{(17b)}$$

The dispersion relation obtained here provides the frequency-wave number dependence for TDLW propagation at any direction inside the x-y plane. This expression is identical to the expression obtained by Vladimirov et al.[17] The dispersion relation is an inverse opticlike dispersion, so the frequency at zero wave number (infinite wavelength) is finite and the slope of the curve $\omega = \omega(k)$ is negative for small k. This information is true for all angles θ, as obvious from Figs. 2(a) and 3. Note that Fig. 3 here is quasi-identical to Fig. 3 in Ref. 16(a) (apart from the difference in scaling and notation).
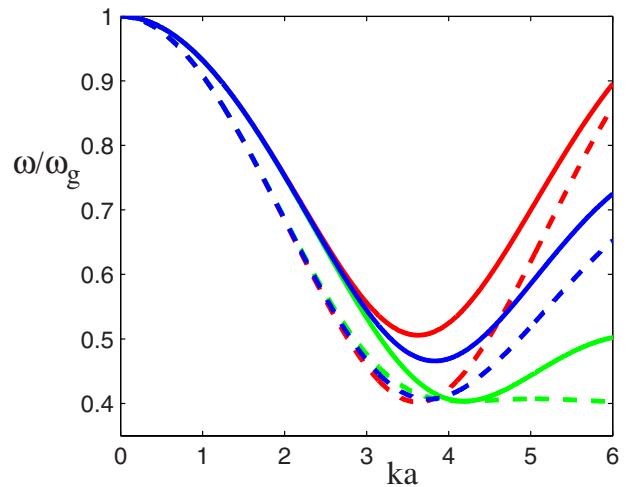

FIG. 3. (Color online) The dispersion relation (36) is plotted (in the collisionless case) for different values of the propagation angle. The solid curves are for FNI while the dashed ones are with SNIs. The angle of propagation is as follows: upper curves: $\theta = 30°$; middle curves: $\theta = 15°$; bottom curves: $\theta = 0$. Note that the solid curves agree perfectly with Fig. 3 in Ref. 16(a).

B. Group velocity

The group velocity of TDLWs (for $\nu = 0$) reads

$$v_g = \frac{a\Omega^2}{\omega}\{\cos\theta\sin[ka\cos\theta]$$

$$+ \cos(\pi/3 - \theta)\sin[ka\cos(\pi/3 - \theta)]$$

$$+ \cos(\pi/3 + \theta)\sin[ka\cos(\pi/3 + \theta)]\}.$$

$$\text{(18)}$$

The dispersion relation presents a negative group velocity for wave numbers k below a threshold, say, $k_{critical}$, and a positive group velocity for $k > k_{critical}$. The value of $k_{critical}$ depends on direction of wave propagation, see Figs. 2(b) and 4. These results are in perfect agreement with the results obtained via numerical simulation.[16] Figure 4 shows a contour plot of the curve $v_g = 0$, which thus determines $k_{critical}$, where
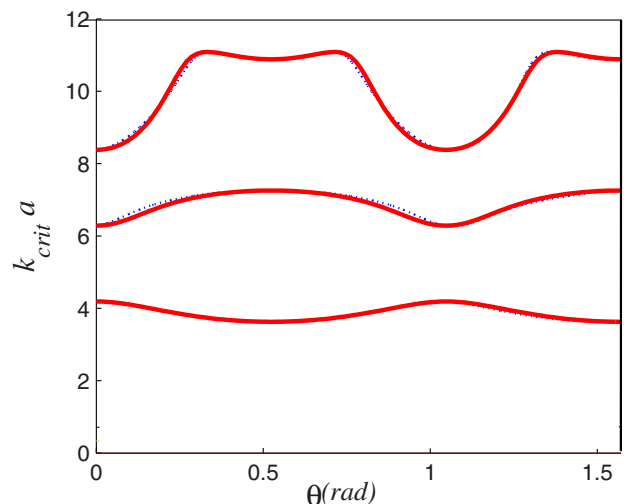

FIG. 4. (Color online) Contour plot of $v_g = 0$ up to FNI. The normalized $k_{critical}$ as a function of θ. The contour plot up to SNI is practically superposed on that for FNI.

the group velocity changes sign as a function of θ. As discussed in Ref. 16(a), the dispersion law in the 2D crystal case differs substantially from the one obtained for 1D crystals. The difference is marked in the form of the dispersion relation (16) and is also in the sign of the group velocity (positive/negative). Our findings recover perfectly those earlier results.

C. Continuum approximation

If the characteristic length scale of the wave form, say, L, is much larger than the interparticle spacing a, then the continuum approximation can be invoked in order to convert the difference [Eq. (11)] into a differential equation for $z_{m,n}$, now expressed as continuous function $u(x,t)$. We expand $z_{m\pm1,n}$ and $z_{m\pm1/2,n\pm\sqrt{3}/2}$ around $z_{m,n}$ in powers of a/L and retain terms of the order of $(a/L)^4$ to obtain

$$z_{m\pm1,n} = z_{m,n} \pm a\frac{\partial u}{\partial x} + \frac{a^2}{2}\frac{\partial^2 u}{\partial x^2} \pm \frac{a^3}{6}\frac{\partial^3 u}{\partial x^3} + \frac{a^4}{24}\frac{\partial^4 u}{\partial x^4} + \cdots,$$

(19)

$$z_{m\pm1/2,n\pm\sqrt{3}/2} = z_{m,n} \pm \frac{a}{2}\frac{\partial u}{\partial x} \pm \frac{\sqrt{3}a}{2}\frac{\partial u}{\partial y} + \frac{a^2}{8}\frac{\partial^2 u}{\partial x^2}$$
$$+ \frac{3a^2}{8}\frac{\partial^2 u}{\partial y^2} \pm \frac{\sqrt{3}a^2}{4}\frac{\partial^2 u}{\partial x\,\partial y} + \cdots.$$

(20)

Substituting from Eqs. (19) and (20) and retaining terms of order in a^4, the equation of motion (11) takes the form of a differential equation for the particle displacement $u_{m,n}(t) \cong u(x,y,t)$,

$$\ddot{u} + \nu\dot{u} = -\omega_g^2 u - K_1 u^2 - K_2 u^3 - \frac{3a^2\Omega^2}{32}[16(u_{xx} + u_{yy})$$
$$+ a^2(u_{xxxx} + u_{yyyy} + 2u_{xxyy})] + \frac{27a^4 K_3}{24}[3(u_x)^2 u_{xx}$$
$$+ 3(u_y)^2 u_{yy} + (u_x)^2 u_{yy} + (u_y)^2 u_{xx} + 4u_x u_y u_{xy}].$$

(21)

Note that the friction term introduced on the left-hand side of the equation of motion (11) and its continuum version (21) lead to the appearance of the damping rate ν (due to dust-neutral collisions) in the dispersion relations (16), (17a), (17b), and (18). Dissipation in dusty plasma experiments is admittedly always present, yet may acquire very small values depending on plasma density and pressure.[26] In the following, we shall assume a very small damping rate and will therefore neglect damping by setting $\nu=0$ in the nonlinear analysis to follow. This is expected to incur a relative error of the order of ν^2/ω_g^2, which is reportedly small in experiments. Our results will later be extended by incorporating dissipation effects omitted here.

III. AMPLITUDE MODULATION AND DYNAMICS— DERIVATION OF A NONLINEAR SCHRÖDINGER EQUATION

We assume that the transverse wave propagates in plane in an arbitrary direction, given by the general form $\hat{x}\cos\theta + \hat{y}\sin\theta$. We shall employ the standard lattice version of the reductive perturbation technique[20,21] in the quasicontinuum limit.

A. A 2D lattice perturbation scheme

Allowing for a weak departure from the small-amplitude (linear) theory, we consider

$$u = \varepsilon u_1 + \varepsilon^2 u_2 + \cdots,$$

(22)

where ε ($\ll1$) is a small (real) parameter characterizing the strength of the nonlinearity. The function u_j at each order is assumed to be a sum of lth order harmonics, viz.,

$$u_j = u_{j0} + \sum_{l=1}^{\infty}\{u_{jl}\exp[il(mk\cos\theta + nk\sin\theta - \omega t)]$$
$$+ \text{c.c.}\},$$

(23)

where c.c. denotes the complex conjugate.

The amplitudes u_{jl} are assumed to be slowly varying function of time and space via the set of independent stretched variables

$$\vec{\xi} = (\hat{x}x_1 + \hat{y}y_1 - v_0 t_1)$$

and

$$\tau = t_2 = \varepsilon t_1.$$

(24)

The analytical expression for the propagation velocity v_0 is anticipated as a compatibility constraint; the outcome is, in fact, expected to yield the group velocity $v_g = \omega(k)$ in the continuum approximation. We shall now substitute these expansions into the equation of motion (21) and collect the contributions appearing in each power in ε.

B. First order—linear dynamics in the continuum limit

At first order, we obtain a linear equation which is solved for the first harmonic solution [cf. Eq. (23) for $l=m=1$; the zeroth-order amplitude vanishes]. The dispersion relation reads

$$\omega^2 = \omega_g^2 - \frac{3k^2 a^2}{2}\Omega^2\left(1 - \frac{k^2 a^2}{16}\right),$$

(25)

which coincides with the dispersion relation (16) in the limit $ka \ll 1$, see Fig. 5.

We note that quite surprisingly, the angle dependence disappears in the dispersion law once the continuum limit $ka \ll 1$ is considered. It is straightforward to verify (upon a simple McLaurin expansion near zero k) that the angle vanishes in the first (five) terms in a small k expansion, and thus
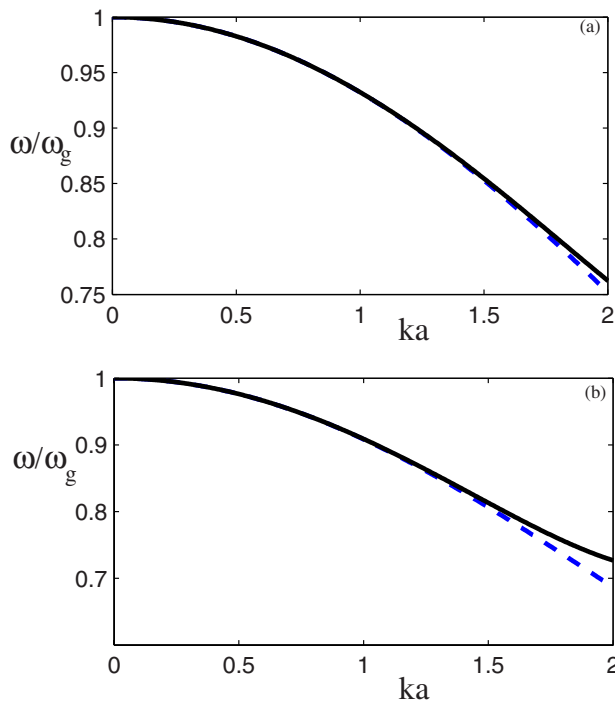
FIG. 5. (Color online) (a) Linear dispersion curve for $\nu=0$ and $\theta=0$; compare the discrete result (dashed line) from Eq. (17a) to the result of the continuum approximation (solid line) from Eq. (25). (b) Same for SNI.

would not appear in any of the quantities to follow herein. Still, we add for rigor that the angle does appear in the algebraic evaluation of the coefficients P and Q below, yet only through combinations of terms which all vanish (upon making use of appropriate trigonometric identities).

C. Second order—group dispersion

In the second order, considering the annihilation of secular terms we obtain the following expression for the propagation velocity v_0:

$$v_0 = -\frac{3ka^2}{2\omega}\Omega^2\left(1 - \frac{k^2a^2}{8}\right). \tag{26}$$

It is easy to verify that $v_0 = v_{g,\text{cont}} = d\omega/dk$, as physically expected. Equation (26), here obtained as a condition for secular term annihilation, can therefore be also derived either from Eq. (25) or as the continuum expansion of Eq. (18) above. The first harmonic u_{11} therefore propagates at the group velocity in a(n) (arbitrary) direction, as suggested by the functional dependence $u_{11} = u_{11}(\xi, \dots)$, where $\xi = \varepsilon(x \cos \theta + y \sin \theta - v_g t)$ here determines the slowly varying amplitude reference frame.

The solution obtained up to this order is given by

$$u_j = \varepsilon(u_{11} \exp i\phi + \text{c.c.}) + \varepsilon^2[u_{20} + (u_{21} \exp i\phi + \text{c.c.})$$
$$+ u_{22} \exp 2i\phi + \text{c.c.}] + O(\varepsilon^3), \tag{27}$$

where the fundamental carrier (first harmonic) phase was denoted by $\phi = k(m \cos \theta + n \sin \theta) - \omega t$. The harmonic amplitudes are given by

$$u_{20} = \frac{-2K_1|u_{11}|^2}{\omega_g^2}, \tag{28}$$

$$u_{22} = \frac{K_1 u_{11}^2}{4\omega^2 - \omega_g^2 + 6k^2a^2\Omega^2(1 - k^2a^2/4)}. \tag{29}$$

Notice the generation of second and zeroth harmonics, which is entirely due to the sheath potential anharmonicity; see that the harmonics only involve (the quadratic force or cubic sheath potential nonlinearity coefficient) K_1, defined in Eq. (12) above; higher-order nonlinearity only affects amplitude dynamics in higher orders, see below. We also note that the zeroth harmonic was found to vanish ($u_{10}=0$) in qualitative agreement with the 1D transverse wave case, see Ref. 21 (and, in fact, in contrast with the 1D longitudinal wave case, see Ref. 20). A detailed qualitative discussion of these matters is carried out in Ref. 15. The above formulation provides a direct tool for harmonic generation related diagnostics to be used in experiments.

D. Third order—NLS equation

In third order in epsilon, the condition for annihilation of secular terms leads to the nonlinear Schrödinger (NLS) equation

$$i\frac{\partial U}{\partial \tau} + P\frac{\partial^2 U}{\partial \xi^2} + QU|U|^2 = 0, \tag{30}$$

which describes the evolution of the fundamental (carrier) harmonic amplitude $u_{11} = u_{11}(\xi, \tau)$ ($\tau = \varepsilon^2 t$ is a slow time scale; the first order space variable ξ was defined above).

The dispersion coefficient P is given by

$$P = \frac{-v_g^2}{2\omega} - \frac{3a^2\Omega^2}{4\omega}\left(1 - \frac{3k^2a^2}{8}\right). \tag{31}$$

Note that P is related to the curvature of the dispersion curve as $P = d^2\omega/2dk^2$, as expected.

The cubic nonlinearity coefficient is due to the nonlinearity induced by the sheath "substrate" potential via K_1 and K_2 and by the electrostatic coupling via K_3. It is given by

$$Q = \frac{1}{2\omega}\left[\frac{4K_1^2}{\omega_g^2} - \frac{2K_1^2}{4\omega^2 - \omega_g^2 + 6\Omega^2 k^2 a^2(1 - k^2a^2/4)} - 3K_2 \right.$$
$$\left. - \frac{27k^4a^4K_3}{8}\right]. \tag{32}$$

Recapitulating, the dynamics of the wave fundamental harmonic amplitude $u_{11} = U(\xi, \tau)$ is governed by the NLS [Eq. (30)] and is thus essentially dynamics by the interplay among the dispersion and nonlinearity coefficients P and Q. Their analytical behavior on relevant parameters will be investigated below once their role in dynamics is briefly summarized in what follows.

IV. EFFECTS OF SECOND NEIGHBOR INTERACTION

In Secs. II and III, we have made the choice to keep only NNIs, hence neglecting longer-range effects. For first principles, this appears to be justified by the fact that the lattice constant is of order of magnitude comparable to the Debye radius, which measures the range of interparticle interactions. On the other hand, electrostatic interactions (albeit screened) are characterized by their long range of action, so one might wonder whether the contribution of longest, e.g., second order, neighbors would play a significant role. Therefore, it appears appropriate to investigate the strength of SNI. Below, we shall show that the addition of SNI in the model certainly provides a small qualitative, yet no major quantitative modification in the dynamics, thus in principle confirming our FNI (first neighbor interaction) result above. We have chosen to dedicate a separate brief section to SNIs in order to trace their influence in a transparent manner. Nevertheless, once the analytical derivation has led us to the anticipated evolution equation for the amplitude [e.g., Eq. (30) above], the analysis will be carried out in Sec. V in parallel, i.e., comparing among the FNI and SNI models.

We shall assume that each particle (m,n) interacts with three pairs of particles, which are located at the sites $(m, n \pm \sqrt{3})$, $(m \pm 3/2, \ n - \sqrt{3}/2)$, and $(m \pm 3/2, \ n + \sqrt{3}/2)$. The distance between the central particle and the second neighbors is $\sqrt{3}a$ in the directions $\theta = \pi/6, \ 3\pi/6, \ 5\pi/6, \ 7\pi/6, \ 9\pi/6,$ and $11\pi/6$. The electrostatic binary interaction force in $z-$ direction F_z exerted on two grains situated at a distance r is derived from a potential function $U(r)$, see Eq. (4) above. By defining $G_1' = (\partial U / \partial r)|_{r = \sqrt{3}a}$ and $G_2' = (\partial^2 U / \partial r^2)|_{r = \sqrt{3}a}$, we can compute the polynomial coefficients G_1' and G_2' for the Yukawa potential. These are

$$G_1' = -\frac{q^2}{4\pi\varepsilon_0\lambda_D^2}(1 + \sqrt{3}\kappa)\frac{\exp(-\sqrt{3}\kappa)}{(\sqrt{3}\kappa)^2} \tag{33a}$$

and

$$G_2' = \frac{q^2}{4\pi\varepsilon_0\lambda_D^3}[2 + 2(\sqrt{3}\kappa) + (\sqrt{3}\kappa)^2]\frac{\exp(-\sqrt{3}\kappa)}{(\sqrt{3}\kappa)^3}. \tag{33b}$$

Now, the discrete lattice equation of motion becomes

$$
\begin{aligned}
\ddot{z}_{m,n} + \nu\dot{z}_{m,n} = &-\omega_g^2 z_{m,n} - K_1 z_{m,n}^2 - K_2 z_{m,n}^3 + \Omega\{[6z_{m,n} - z_{m+1,n} - z_{m-1,n} - z_{m+1/2,n+\sqrt{3}/2} - z_{m+1/2,n-\sqrt{3}/2} - z_{m-1/2,n+\sqrt{3}/2} \\
&- z_{m-1/2,n-\sqrt{3}/2}] + \alpha[6z_{m,n} - z_{m,n+\sqrt{3}} - z_{m,n-\sqrt{3}} - z_{m+3/2,n+\sqrt{3}/2} - z_{m+3/2,n-\sqrt{3}/2} - z_{m-3/2,n+\sqrt{3}/2} - z_{m-3/2,n-\sqrt{3}/2}]\} \\
&+ K_3\{[(z_{m+1,n} - z_{m,n})^3 + (z_{m-1,n} - z_{m,n})^3 + (z_{m+1/2,n+\sqrt{3}/2} - z_{m,n})^3 + (z_{m+1/2,n-\sqrt{3}/2} - z_{m,n})^3 + (z_{m-1/2,n+\sqrt{3}/2} - z_{m,n})^3 \\
&+ (z_{m-1/2,n-\sqrt{3}/2} - z_{m,n})^3] + \beta[(z_{m,n+\sqrt{3}} - z_{m,n})^3 + (z_{m,n-\sqrt{3}} - z_{m,n})^3 + (z_{m+3/2,n+\sqrt{3}/2} - z_{m,n})^3 + (z_{m+3/2,n-\sqrt{3}/2} - z_{m,n})^3 \\
&+ (z_{m-3/2,n+\sqrt{3}/2} - z_{m,n})^3 + (z_{m-3/2,n-\sqrt{3}/2} - z_{m,n})^3]\},
\end{aligned}
\tag{34}
$$

where the parameters $\alpha = G_1'/\sqrt{3}G_1$ and $\beta = [G_1' - (\sqrt{3}a)G_2']/[3\sqrt{3}(G_1 - G_2 a)]$ represent the second neighbor contribution. Combining with Eqs. (33) and (34) above, the SNI parameters are given by

$$\alpha = \frac{1}{3\sqrt{3}}\left(\frac{1 + \sqrt{3}\kappa}{1 + \kappa}\right)\exp[-\kappa(\sqrt{3} - 1)] \tag{35a}$$

and

$$\beta = \frac{1}{3\sqrt{3}}\left(\frac{1 + \sqrt{3}\kappa + \kappa^2}{3 + 3\kappa + \kappa^2}\right)\exp[-\kappa(\sqrt{3} - 1)]. \tag{35b}$$

Obviously, the FNI expressions above are recovered in the limit $\alpha = \beta = 0$. Figure 6 shows the parameters α and β as a function of κ. We stress the fact that they both take small values (of the order of 0.1 or less approximately) in the region of experimental interest (κ values near unity) *a priori*

suggesting a small contribution by SNIs.

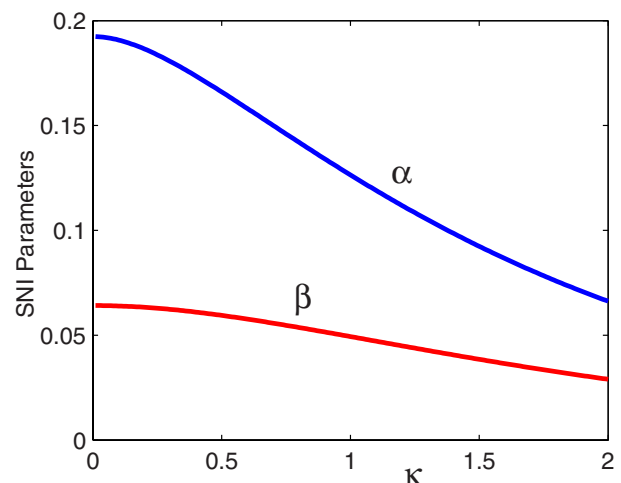The linear dispersion relation [cf. Eq. (16) above] now becomes

FIG. 6. (Color online) The parameters α and β (effect of SNI) as a function of κ.

$$\omega^2 + i\nu\omega = \omega_g^2 - 4\Omega^2 \left\{ \sin^2\left[\frac{ka}{2}\cos\theta \right] + \sin^2\left[\frac{ka}{2}\cos\left(\frac{\pi}{3} - \theta\right) \right] + \sin^2\left[\frac{ka}{2}\cos\left(\frac{\pi}{3} + \theta\right) \right] \right\}$$
$$- 4\Omega^2\alpha \left\{ \sin^2\left[\frac{\sqrt{3}ka}{2}\sin\theta \right] + \sin^2\left[\frac{\sqrt{3}ka}{2}\cos\left(\frac{\pi}{6} - \theta\right) \right] + \sin^2\left[\frac{\sqrt{3}ka}{2}\cos\left(\frac{\pi}{6} + \theta\right) \right] \right\}. \tag{36}$$

Note that only the linear SNI contribution via α enters the dispersion relation. Setting $\nu=0$ to continue (see discussion above), we now advance to the TDLW group velocity to find

$$v_g = \frac{a\Omega^2}{\omega}\{\cos\theta\sin[ka\cos\theta] + \cos(\pi/3 - \theta)\sin[ka\cos(\pi/3 - \theta)] + \cos(\pi/3 + \theta)\sin[ka\cos(\pi/3 + \theta)]\}$$
$$- \frac{\sqrt{3}a\Omega^2}{\omega}\alpha\{\sin\theta\sin[\sqrt{3}ka\sin\theta] + \cos(\pi/6 - \theta)\sin[\sqrt{3}ka\cos(\pi/6 - \theta)] + \cos(\pi/6 - \theta)\sin[\sqrt{3}ka\cos(\pi/6 - \theta)]\}. \tag{37}$$

Again, as expected, expression (18) is recovered in the appropriate limit. On the other hand, in the long-wavelength region (for $ka \ll 1$) one obtains an approximate expression that recovers expression (26) above for $\alpha=0$. This continuum approximation of Eq. (37) need not be stated here, as it is exactly identical to the expression (40) for the propagation velocity v_0 derived below as a compatibility constraint.

Recall that the continuum approximation allowed us to pass from Eq. (11) to Eq. (21) above. The same procedure now yields the SNI-modified continuous equation of motion

$$\ddot{u} + \nu\dot{u} = -\omega_g^2 u - K_1 u^2 - K_2 u^3 - \frac{3a^2\Omega^2}{32}[16(u_{xx} + u_{yy})$$
$$\times (1 + 3\alpha) + a^2(u_{xxxx} + u_{yyyy} + 2u_{xxyy})(1 + 9\alpha)]$$
$$+ \frac{27a^4 K_3'}{24}[3(u_x)^2 u_{xx} + 3(u_y)^2 u_{yy} + (u_x)^2 u_{yy}$$
$$+ (u_y)^2 u_{xx} + 4u_x u_y u_{xy}], \tag{38}$$

where $K_3' = K_3(1 + 9\beta)$. Equation (38) is to be compared with Eq. (21), which is indeed recovered in the appropriate limit. We note that the modification due to SNI being taken into account is only quantitative (slight modification of coefficients) rather than qualitative [no structural modification in Eq. (38) as compared to Eq. (21)] and is expected to be rather weak (as indeed confirmed by the plots below).

At first order, we obtain a linear equation that is solved for the first harmonic solution. The dispersion relation reads

$$\omega^2 = \omega_g^2 - \frac{3k^2 a^2}{2}\Omega^2\left[(1 + 3\alpha) - \frac{k^2 a^2}{16}(1 + 9\alpha) \right], \tag{39}$$

which coincides with the dispersion relation (36) in the limit $ka \ll 1$ (and switching off damping therein).

In the second order, imposing the annihilation of secular terms, we obtain the following expression for the propagation velocity v_0:

$$v_0 = -\frac{3ka^2}{2\omega}\Omega^2\left[1 + 3\alpha - \frac{k^2 a^2}{8}(1 + 9\alpha) \right]. \tag{40}$$

In third order in epsilon, the condition for annihilation of secular terms leads exactly to the NLS [Eq. (30)] above. We recall that it describes the evolution of the envelope (of the fundamental harmonic amplitude) $u_{11} = u_{11}(\xi, \tau)$. The difference now, SNI being taken into account, lies in the modification of the form of the coefficients appearing in Eq. (30). The modified dispersion coefficient P is now given by

$$P = \frac{-v_g^2}{2\omega} - \frac{3a^2\Omega^2}{4\omega}\left[1 + 3\alpha - \frac{3k^2 a^2}{8}(1 + 9\alpha) \right]. \tag{41}$$

Note that P is again related to the curvature of the dispersion curve as $P = d^2\omega/2dk^2$, as expected [and indeed verified upon a double differentiation of Eq. (39) or of Eq. (36) in the continuum limit]. The cubic nonlinearity coefficient with the effect of SNI is now given by

$$Q = \frac{1}{2\omega}\left\{ \frac{4K_1^2}{\omega_g^2} \right.$$
$$- \frac{2K_1^2}{4\omega^2 - \omega_g^2 + 6\Omega^2 k^2 a^2[1 + 3\alpha - k^2 a^2(1 + 9\alpha)/4]}$$
$$\left. - 3K_2 - \frac{27k^4 a^4 K_3'}{8} \right\}, \tag{42}$$

where the SNI influence is manifested via the appearance of α and β—the latter via $K_3' = K_3(1 + 9\beta)$ (as defined above).

V. MODULATIONAL INSTABILITY—2D ENVELOPE EXCITATIONS

The amplitude dynamics of a TDLW packet was shown to be governed by the NLS [Eq. (30)] above. Two physical phenomena that are generally modeled via this formulation are wave collapse via modulational instability and the formation of envelope excitations. Without reproducing the whole of the existing theory, which may be found, for e.g., in Ref. 27 (also in Refs. 21 and 22), we shall provide the basic information needed to understand our findings in what follows.

The detailed analysis of the NLS [Eq. (30)] above[18,19,26] reveals that a modulated wave packet whose amplitude obeys the NLS equation [Eq. (30)] is modulationally unstable for $PQ > 0$ and stable for $PQ < 0$. Assuming a perturbation of amplitude Ψ_0 and characteristic wave number $\tilde{k}$, the perturbation grows $PQ > 0$ leading to wave blowup. The maximum growth rate $\sigma = Q|\Psi_0|^2$ is attained for a perturbation wave number

$$\tilde{k} = \left(\frac{2Q}{P}\right)^{1/2} |\Psi_0|.$$

The coefficients P and Q therefore determine the occurrence and first stage evolution of the instability.

Only the first evolution stage of the instability outlined above can be described analytically. The further evolution of the instability can only be modeled numerically. It is known that energy occurs via the formation of localized envelope structures (*envelope solitons*). In the case $PQ > 0$, *bright-type solitons* are formed: these model localized envelope pulses, which confine the fast carrier wave and move at or near the group velocity, and are formally equivalent to bright pulses in nonlinear fiber optics. On the other hand, for $PQ < 0$, modulated wave packets may propagate in the form of *dark/gray envelope solitons*, modeling localized voids amidst constant values everywhere else.

In an attempt to go one step beyond the continuum approximation adopted above, we shall consider in our analysis, for the sake of rigor, two versions of the dispersion coefficient P, namely, $P_1 = P_{cont}$, as defined (in the continuum limit) in Eq. (31), and the exact (discrete) expression $P_0 = P_{disc} = d^2\omega/2dk^2$, as obtained from the accurate dispersion relation in Eq. (16). Figure 7(a) (solid line) shows the variation in the dispersion coefficient P in the discrete description as obtained from the dispersion relation (for $\nu = 0$) for FNI [Eq. (16)] on one hand (solid curves; notice the 4π-periodicity) and separately for SNI from Eq. (36) on the other (dashed curves). The continuous and discrete descriptions obviously coincide in the low wave number k limit, yet diverge strongly for larger k (shorter wavelengths), compare Fig. 7(a) to Fig. 9 near $k \approx 0$ to see this. This twofold analysis (continuous versus discrete and FNI versus SNI) is meant to give a flavor of what should be an accurate discrete-system investigation, which is to follow in future work.

The behavior of the coefficients P and Q are depicted in Fig. 7. The product PQ and also the ratio Q/P are depicted in Fig. 8. Recalling that the sign of the product PQ determines the stability profile of the wave, we see that the occurrence of modulational instability is prescribed, since both P and Q are negative (hence, $PQ > 0$). Stable bright-type envelope structures should therefore be sustained in the system. Indeed, this prediction seems to have been confirmed already in the laboratory, where the observation of backward propagating wave packets is reported and their characteristics are tested against a linear theory, which are thus confirmed in the 2D picture. It must be added for rigor that the
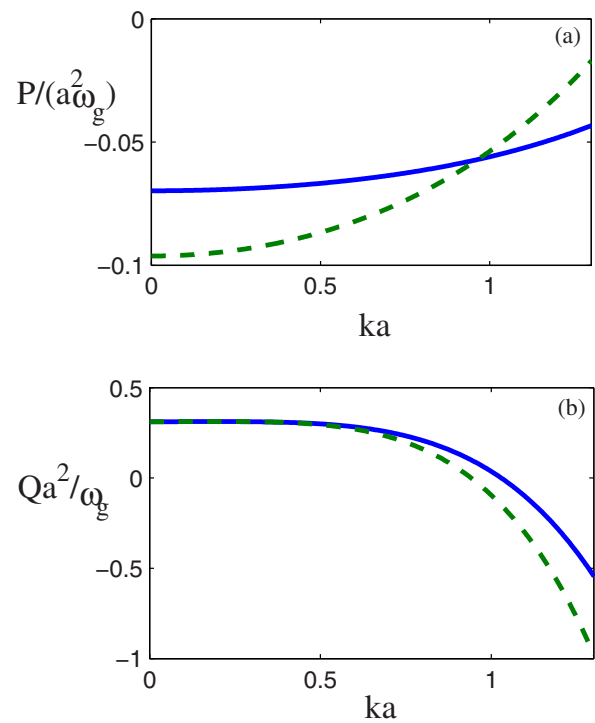

FIG. 7. (Color online) Variation in (a) the coefficient P up to FNI (solid line) and up to SNI (dashed lines) in the continuous model as a function of ka. (b) The coefficient Q (continuous) as a function of ka.
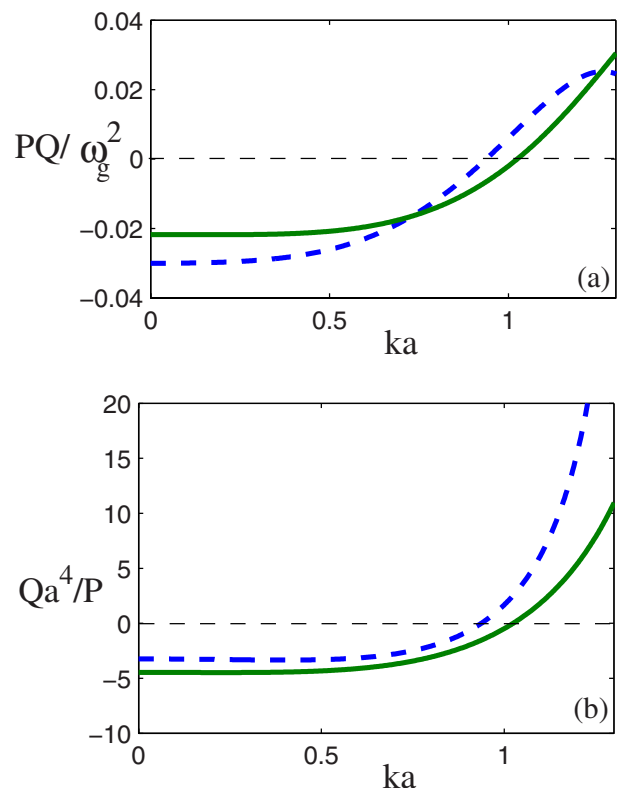

FIG. 8. (Color online) Variation in (a) the product of coefficients PQ (continuous) up to FNI (solid lines) and up to SNI (dashed lines) as a function of ka. (b) The ratio of coefficients Q/P (continuous) as a function of ka (solid lines for FNI and dashed lines for SNI).

sign of P (and presumably Q) may change by taking into account SNI, thus affecting the stability profile of modulated wave packets, and the type of envelope solitons susceptible to occur.

A. Continuum versus discrete

It must be stated for rigor that the above findings are only true for low k (within the continuum approximation here), i.e., for large wavelengths, say, $\lambda \gg r_0$ [the region below $k \approx r_0^{-1}$ seems to be satisfactorily covered by the continuum approximation within an error of 10%, see Fig. 7(a)]. For higher k, the dispersion coefficient P (in fact, 4π-periodic) changes sign and Q may presumably also do the same. Properly speaking, Q [see Fig. 7(b)] does become positive above $k \approx 1.1 r_0^{-1}$ (for FNI) and $k \approx 0.85 r_0^{-1}$ (for SNI), yet this is expected to change if a discrete analysis were to be undertaken. In general, it seems safe to assert that a more complex stability profile will be predicted by a more accurate discrete analysis; in particular, wave packets will be stable (and dark-type envelope excitations will occur) at wave numbers higher than $k \approx r_0^{-1}$, as suggested by Fig. 7. Concluding therefore, we stress that one needs to go into a fully discrete description of dust crystal dynamics in order to obtain a valid expression for the nonlinearity coefficient Q (P on the other hand is readily obtained from the dispersion law, as explained above). This is anticipated as part of a future investigation yet goes beyond the continuum approximation adopted here.

B. FNI versus SNI

Summarizing the overall effect of taking SNIs into account, we note that it appears to be small yet rather non-negligible. The dispersion laws certainly undergo a modification: the frequency is reduced by (near or less than) 20% (see Fig. 3), while a small effect is also observed in the critical wave number threshold where the slope changes from negative (backward wave) to positive (forward propagation); note the positions of the minimae in Fig. 3. Obviously this also affects the group velocity and group velocity dispersion terms (see, e.g., Fig. 9 for P); nevertheless this remark is rather not relevant in the continuous (small k) region (modeled by our NLS equation here) as explained above. Interestingly, for propagation parallel to the lattice principal axes, SNIs may account for slowing down a wave with a short wavelength (k higher than 4, roughly), and thus the backward wave character may be modified in a critical manner; compare the bottom two curves (in green, online) to see this: the slope of the dashed one essentially goes horizontally after $ka = 4$ approximately. To be stated again, this enters a region (of high k values) which goes beyond the continuum approximation adopted here. This is entirely legitimate in the linear regime, yet no prediction is in principle to be made in the nonlinear region (involving the NLS equation coefficients, say, P and Q).
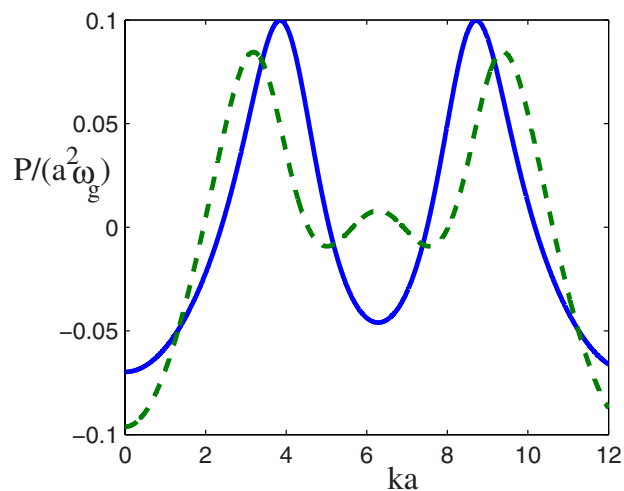

FIG. 9. (Color online) Variation in the dispersion coefficient P in the discrete description as a function of ka (solid line) obtained from the dispersion relation up to FNI [Eq. (16) for $\nu = 0$] and (dashed line) up to SNI [Eq. (36)]. Notice the 4π-periodicity.

VI. CONCLUSIONS

The amplitude modulation of transverse off-plane DL wave packets in 2D hexagonal dusty plasma crystals has been investigated. The modulational instability predicted by our findings may be seen as a first stage of the out-of-plane lattice instability observed numerically[16] and might presumably lead to the phase transition suggested in the latter reference. Modulational instability may also be the first stage of the generic (i.e., for any symmetric potential) structural instability suggested in Ref. 23. We need to point out for rigor that the modulation theory employed here is a mildly nonlinear theory, which is only valid for weak vertical displacements. The latter point justifies our choice in neglecting the coupling to in-plane dust grain motion, since we are only interested in the very first stage of the manifestation of nonlinearity in off-plane motion. A more general theory should take into account horizontal-to-vertical motion coupling and should be the subject of forthcoming work of ours.

The linear dispersion characteristics of transverse DL waves were studied, including the dispersion relation, group velocity, and an evolution equation for the modulated amplitude of the first harmonic was derived. The dispersion relation shows a negative group velocity of the wave for $k < k_{\text{critical}}$ and a positive group velocity for $k > k_{\text{critical}}$. The value of k_{critical} depends on the direction of wave propagation. These results are in excellent agreement with earlier numerical,[16] experimental,[5] and theoretical[17] results.

We have relied on a 2D lattice multiple scale theory to separate the slow envelope evolution scale from the fast carrier space/time scales and investigate the amplitude dynamics. We have shown that transverse wave packets will in principle be stable in the long wavelength region, although modulational instability for shorter wavelengths is in principle not to be excluded (yet to be covered by a discrete version of the model to come). Furthermore, we predict the formation of both bright and dark-type envelope solitons in regions similar to the bright envelope structures observed in

laboratory experiments.[5] Admittedly, our study was limited within the continuum approximation; thus our results are valid in the long-wavelength limit. Therefore, rigorously speaking, only the small (wave number) k region of our plots should be retained in a strictly quantitative interpretation. Nevertheless, we can anticipate a discrete version of the theory, which would incorporate a discrete form of the NLS coefficients P (known, from the discrete dispersion relation) and Q (unknown, to be determined). Our graphs seem to suggest that both coefficients may change sign for higher k (shorter wavelength), hence allowing for a richer dynamical profile (beyond the continuum limit).

Furthermore, in an attempt to determine the region of validity of our study, in as much rigor as possible, we have investigated the role of the interaction among grains located at second neighbor sites. We have shown that this effect is rather small (compared to first neighbor interactions) as more or less expected physically; recall that the lattice spacing is of comparable order of magnitude to the Debye sphere in these strongly coupled configurations. However, longer than NNIs may give rise to interesting phenomena, as in particular a modification of the system's behavior from the backward to the forward wave regime, as discussed in the text (see Fig. 3). Finally, we may add that although energy dissipation was neglected in this investigation, it may be added at a later stage. Physical effects thus predicted are quite distinct, as shown by preliminary studies, so our aim was to pinpoint the difference by addressing the damped wave case separately in forthcoming work.

Our work is of relevance in dusty plasma crystal experiments in the laboratory, where our predictions for the type and stability of modulated wave packets can be tested and will hopefully be confirmed. Beyond dusty (complex) plasma physics, we view this work as a fundamental investigation of nonlinear transverse motion in hexagonal crystals of potential relevance (either currently or in the future) in other physical contexts, where electrostatic-interaction-sustained crystalline structures occur (such as ultracold plasmas or one-component plasmas), or in lattice theory and in discrete dynamical systems where pulse formation and wave packet localization occur.

ACKNOWLEDGMENTS

[1] P. K. Shukla and A. A. Mamun, *Introduction to Dusty Plasma Physics* (Institute of Physics, Bristol, 2002).

[2] S. V. Vladimirov, K. Ostrikov, and A. Samarian, *Physics and Applications of Complex Plasmas* (Imperial College Press, London, 2005).

[3] G. Morfill, H. M. Thomas, and M. Zuzic, in *Advances in Dusty Plasmas*, edited by P. K. Shukla, D. A. Mendis, and T. Desai (World Scientific, Singapore, 1997), pp. 99–142.

[4] H. Thomas, G. E. Morfill, V. Demmel, J. Goree, B. Feuerbacher, and D. Mohlmann, Phys. Rev. Lett. **73**, 652 (1994).

[5] D. Samsonov, S. Zhdanov, and G. Morfill, Phys. Rev. E **71**, 026410 (2005).

[6] A. Homann, A. Melzer, S. Peters, and A. Piel, Phys. Rev. E **56**, 7138 (1997).

[7] T. Misawa, N. Ohno, K. Asano, M. Sawai, S. Takamura, and P. K. Kaw, Phys. Rev. Lett. **86**, 1219 (2001); B. Liu and J. Goree, Phys. Rev. E **71**, 046410 (2005).

[8] F. Melandso, Phys. Plasmas **3**, 3890 (1996).

[9] S. V. Vladimirov, P. V. Shevchenko, and N. F. Cramer, Phys. Rev. E **56**, R74 (1997).

[10] S. V. Vladimirov, P. V. Shevchenko, and N. F. Cramer, Phys. Plasmas **5**, 4 (1998).

[11] R. Kompaneets, A. V. Ivlev, V. Tsytovich, and G. Morfill, Phys. Plasmas **12**, 062107 (2005); R. Kompaneets, U. Konopka, A. V. Ivlev, V. Tsytovich, and G. Morfill, *ibid.* **14**, 052108 (2007).

[12] E. B. Tomme, D. A. Law, B. M. Annaratone, and J. E. Allen, Phys. Rev. Lett. **85**, 2518 (2000).

[13] G. Sorasio, R. A. Fonseca, D. P. Resendes, and P. K. Shukla, *Dust Plasma Interactions in Space* (Nova, New York, 2002), pp. 37–70.

[14] V. Koukouloyannis and I. Kourakis, Phys. Rev. E **76**, 016402 (2007).

[15] I. Kourakis and P. K. Shukla, Int. J. Bifurcation Chaos Appl. Sci. Eng. **16**, 1711 (2006).

[16] K. Qiao and T. W. Hyde, Phys. Rev. E **68**, 046403 (2003); J. Phys. A **36**, 6109 (2003); Z. Donkó, P. Hartmann, and G. J. Kalman, Phys. Rev. E **69**, 065401(R) (2004).

[17] S. V. Vladimirov, V. V. Yaroshenko, and G. E. Morfill, Phys. Plasmas **13**, 030703 (2006).

[18] B. Farokhi, I. Kourakis, and P. K. Shukla, Phys. Plasmas **13**, 122304 (2006).

[19] M. Remoissenet, *Waves Called Solitons*, 2nd ed. (Springer-Verlag, Berlin, 1996).

[20] A. Hasegawa, *Plasma Instabilities and Nonlinear Effects* (Springer-Verlag, Berlin, 1975).

[21] I. Kourakis and P. K. Shukla, Phys. Plasmas **11**, 1384 (2004).

[22] I. Kourakis and P. K. Shukla, Phys. Plasmas **11**, 2322 (2004); **11**, 3665 (2004).

[23] D. N. Klochkov and N. G. Gusein-zade, Plasma Phys. Rep. **33**, 646 (2007).

[24] U. Konopka, G. E. Morfill, and L. Ratke, Phys. Rev. Lett. **84**, 891 (2000).

[25] A. V. Ivlev, R. Sutterlin, V. Steinberg, M. Zuzic, and G. Morfill, Phys. Rev. Lett. **85**, 4060 (2000).

[26] D. Samsonov, personal communication (2009).

[27] T. Dauxois and M. Peyrard, *Physics of Solitons* (Cambridge University Press, Cambridge, 2006).